










Cite this: *Soft Matter*, 2023, 19, 5942

## Multiscale investigation of viscoelastic properties of aqueous solutions of sodium alginate and evaluation of their biocompatibility

Alberto Varela-Feijoo, <sup>af</sup> Philippe Djemia, <sup>b</sup> Tetsuharu Narita, <sup>c</sup> Frédéric Pignon, <sup>d</sup> Armelle Baeza-Squiban, <sup>e</sup> Valentina Sirri <sup>e</sup> and Alain Ponton <sup>\*a</sup>

In order to get better knowledge of mechanical properties from microscopic to macroscopic scale of biopolymers, viscoelastic bulk properties of aqueous solutions of sodium alginate were studied at different scales by combining macroscopic shear rheology (Hz), diffusing-wave spectroscopy microrheology (kHz–MHz) and Brillouin spectroscopy (GHz). Structural properties were also directly probed by small-angle X-ray scattering (SAXS). The results demonstrate a change from polyelectrolyte behavior to neutral polymer behavior by increasing polymer concentration with the determination of characteristic sizes (persistence length, correlation length). The viscoelastic properties probed at the phonon wavelength much higher than the ones obtained at low frequency reflect the variation of microscopic viscosity. First experiments obtained by metabolic activity assays with mouse embryonic fibroblasts showed biocompatibility of sodium alginate aqueous solutions in the studied range of concentrations (2.5–10 g L<sup>-1</sup>) and consequently their potential biomedical applications.

Received 9th February 2023,  
Accepted 11th July 2023

DOI: 10.1039/d3sm00159h

[rsc.li/soft-matter-journal](http://rsc.li/soft-matter-journal)

### 1. Introduction

Sodium alginate is the sodium salt of a naturally-occurring polysaccharide present in the skeleton of brown algae<sup>1</sup> such as *Laminaria hyperborea*, *Laminaria digitata* and *Macrocystis pyrifera*, with a structural function similar to that of cellulose in land plants. It is a copolymer composed of linear unbranched blocks of  $\beta$ -D-mannuronic acid (M block),  $\alpha$ -L-guluronic acid (G block) or alternating (MG block) covalently linked by (1,4) – glycosidic linkage.<sup>2,3</sup> The carboxylic groups presented in both monomers lead to negative charges along the backbone, which confer a polyelectrolyte nature and strongly influence its properties in aqueous solutions. In addition, alginates stand out due to the chemical structure of rigid monomers of

six-membered sugar rings connected by glycosidic linkages with restricted rotation. These lead to stiffer chains with high hydrophilicity and then, highly interconnected entangled networks in aqueous solution at relatively low concentrations and moderate chain contour length. Beyond multiple applications in the food, cosmetics, textile and pharmaceutical industry, its ability to interact with divalent cations (*e.g.*, Ca<sup>2+</sup>), producing biocompatible hydrogels with tunable mechanical properties in the range of different kinds of living tissues, make them excellent candidates for biomedicine in wound healing, drug delivery and tissue engineering applications.<sup>4</sup>

As a general characteristic of naturally derived materials, the properties of alginate depend on the source: the chemical composition and sequence of monomers may vary widely between algae species and even between different parts of the algae and the time of year when it is harvested.<sup>5</sup> This variable chemical composition and structure of alginates have noticeable effects on some of their relevant properties such as the viscosity in solution, the interactions with divalent cations or the biocompatibility.<sup>6</sup> The main explanation is the different degrees of hindered rotation around the glycosidic linkages connecting the monomers depending on the block type (M block, G block or MG block) leading to higher stiffness in the order GG > MM > MG.<sup>7</sup> Then, alginates with higher content of G block will be composed of more rigid chains with a more expanded conformation and higher viscosities in

<sup>a</sup> Laboratoire Matière et systèmes complexes (MSC), Université Paris Cité et CNRS, UMR 7057, 10 rue A. Domon et L. Duquet, 75013 Paris, France.

E-mail: [alain.ponton@u-paris.fr](mailto:alain.ponton@u-paris.fr)

<sup>b</sup> Laboratoire des Sciences des procédés et des matériaux (LSPM), UPR-CNRS 3407, 99 Avenue Jean-Baptiste Clément, 93530 Villetaneuse, France

<sup>c</sup> École supérieure de physique et de chimie industrielles de la ville de Paris (ESPCI), 10 Rue Vauquelin, 75005 Paris, France

<sup>d</sup> Laboratoire rhéologie et procédés (LPG) Université Grenoble Alpes, CNRS, UMR 5520, Domaine Universitaire, BP 53, 38041 Grenoble Cedex 9, France

<sup>e</sup> Unité de Biologie fonctionnelle et adaptative (BFA), Université Paris Cité et CNRS, UMR 8251, 4 rue Marie-Andrée Lagroua Weill-Hallé, 75013 Paris, France

<sup>f</sup> Université Paris Saclay, INRAE, AgroParisTech, UMR SayFood, 91120 Palaiseau, France



aqueous solutions.<sup>8</sup> High G content favors the interactions with bivalent cations allowing to obtain stiffer hydrogels.<sup>9</sup> It has also been shown that low M/G ratio and high molecular weight alginates have better biocompatibility and fewer immunological reactions during implantation.<sup>10,11</sup>

The understanding of these variable properties has attracted the attention of numerous researches in the last decades leading to a complete characterization of the molecular structure of a wide range of sodium alginates of different origins<sup>5</sup> and different extraction conditions.<sup>12</sup> The classical parameters that can contribute to easily identify the expected properties of a given alginate product are their molecular weight<sup>13</sup> and ratio M/G.<sup>14</sup> However, they are not enough to unambiguously define the molecular structure of a copolymer and the sequential structure of the alginate chains was completely determined by more time-consuming and costly techniques such as nuclear magnetic resonance (NMR)<sup>15,16</sup> to get a better understanding of the properties of the alginate.<sup>6</sup> If a lot of the studies are focused on the implications of this complex chemical structure on the properties of alginate hydrogels,<sup>17–19</sup> the situation is less complete with regard to the rheological behavior of sodium alginate solutions at different concentrations.

The interest of the bulk rheological properties of the sodium alginate solutions lies in their direct relation not only to the microscopic parameters of individual chains but also to the interactions between chains (entanglements). The charges play a key role through the strong intra- and inter- electrostatic repulsions especially relevant in salt-free or low-salt aqueous solutions. The complexity of these electrostatic interactions still raises many open questions. The dynamics of polyelectrolytes are controlled by a combination of different relaxation processes at different structural levels over a wide time or frequency scale. However, most of the rheological studies performed on sodium alginate are limited to the range covered by conventional rotational rheometers (<10<sup>2</sup> Hz).<sup>20–29</sup> Time-temperature superposition is not suitable to extend this frequency range for alginate solutions and even if optical techniques<sup>30</sup> have become increasingly available covering broader frequency ranges, only one study has explored the high-frequency behavior of sodium alginate solutions<sup>31</sup> to the best of our knowledge. Nevertheless, the study of the rheological properties of sodium alginate in a broader frequency range is of major importance not only to find some relations with the molecular structure but also for the modulation of the physicochemical features for many of their challenging biomedical applications. Some examples could be the modulation of the interactions with other constituents during the elaboration of nanomaterials<sup>32</sup> or hybrid hydrogels and the adjustment of the transient liquid properties required for injectable *in situ* forming<sup>33</sup> or 3D printing<sup>34</sup> alginate hydrogels.

In this context, we propose a global strategy by combining macroscopic shear rheology (Hz), diffusing-wave spectroscopy microrheology (kHz–MHz) and Brillouin spectroscopy (GHz) in order to investigate the viscoelastic bulk properties of aqueous solutions of sodium alginate in a wide frequency domain. This multiscale study will make possible to extend the characterization of the rheology and the dynamics of the network beyond the frequency-range of the studies available in the literature.

In addition, small-angle X-ray scattering (SAXS) experiments are performed to probe directly the structural properties. In view of the potential biomedical applications of alginate matrices, first preliminary results on biocompatibility are also presented.

## 2. Experimental

### 2.1. Aqueous solutions of sodium alginate

The selected sodium alginate for this study is an alginic acid sodium salt of low viscosity (MP Biomedicals) extracted from brown seaweed *Macrocystis pyrifera*. It consists in a cream-colored powder with a small amount of humidity (8%) determined by measuring the mass before and after 24 hours in an oven at 80 °C. A mother aqueous solution of sodium alginate (40 g L<sup>-1</sup>) was prepared by weighing the proper amount of alginate powder and dissolving in pure water by mechanical stirring (400 rpm) for 14 hours. All the analyzed aqueous solutions of sodium alginate with a concentration ranging between 0.1 and 40 g L<sup>-1</sup> were prepared by diluting this mother solution in pure water and mixing by mechanical stirring until the sample becomes homogeneous. For concentrations between 0.1 and 2 g L<sup>-1</sup>, a set of samples was prepared in water with added salt (NaCl 0.1 M) to screen the electrostatic repulsions of negatively charged sodium alginate chains.

### 2.2. Microrheology

A torque-controlled rheometer (MARS) with a cone-plate titanium geometry (diameter of 60 mm, angle of 1°, gap of 51.2 μm) was used to carry out all the microrheological measurements. Temperature control was achieved by a Peltier device located in the base of the geometry. For diluted solutions of sodium alginate, below 2 g L<sup>-1</sup>, the Newtonian viscosity was determined by steady-state shear flow measurements in a range of shear rates between 200 and 500 s<sup>-1</sup>. Each measurement was done in triplicate and the shown results correspond to a mean over the three experimental values. For concentrated aqueous solutions of sodium alginate, between 2 and 40 g L<sup>-1</sup>, the shear-dependence of the viscosity was determined by steady-state shear flow measurements between 0.1 and 2000 s<sup>-1</sup>. In addition, oscillatory frequency sweeps between 0.01 and 100 Hz were performed with a fixed strain of 1% within the linear viscoelastic domain (LVD) for the concentrations 14, 20, 24 and 32 g L<sup>-1</sup> for the comparison with microrheological measurement.

### 2.3. DWS-based microrheology

Microrheological measurements based on diffusing-wave spectroscopy (DWS) were performed using a laboratory-made setup described in detail in a previous paper.<sup>35</sup> The coherent source was a Spectra-Physics Cyan CDRH laser, operated at λ = 488 nm with an output power of 50 mW. The laser beam was expanded to approximately 1 cm at the sample. The scattered light was collected by a photon counter system and analyzed to obtain the intensity autocorrelation function. Alginate samples for DWS measurements were prepared in cuvettes for fluorescence spectroscopy (L = 4 mm in path length).



Spherical microparticles of polystyrene ( $\varnothing = 500$  nm) covered with alkyl-OH surface (MICROMOD) were dispersed in the alginate solutions with a concentration of 1% w/w. The mixtures were stable, and no aggregation or precipitation was observed macroscopically for all the solutions tested in this work.

The obtained intensity autocorrelation function  $g^{(2)}(t)$  was converted into the field autocorrelation function  $g^{(1)}(t)$  by the Siegert relation,  $g^{(2)}(t) = 1 + \beta [g^{(1)}(t)]^2$ ,  $\beta$  being about 0.72. Then, the mean square displacement (MSD =  $\langle \Delta r^2(t) \rangle$ ) was calculated by solving numerically the following equation:<sup>35</sup>

$$g^{(1)}(t) = \left[ \frac{L}{l^*} + \frac{4}{3} \right] / \left\{ \left[ \frac{z_0}{l^*} + \frac{2}{3} \right] \times \left\{ \sin h \left[ \frac{z_0}{l^*} \sqrt{k_0^2 \langle \Delta r^2(t) \rangle} \right] + \frac{2}{3} \sqrt{k_0^2 \langle \Delta r^2(t) \rangle} \cos h \left[ \frac{z_0}{l^*} \sqrt{k_0^2 \langle \Delta r^2(t) \rangle} \right] \right\} / \left\{ \left( 1 + \frac{4}{9} k_0^2 \langle \Delta r^2(t) \rangle \right) \times \sin h \left[ \frac{L}{l^*} \sqrt{k_0^2 \langle \Delta r^2(t) \rangle} \right] + \frac{2}{3} \sqrt{k_0^2 \langle \Delta r^2(t) \rangle} \cos h \left[ \frac{L}{l^*} \sqrt{k_0^2 \langle \Delta r^2(t) \rangle} \right] \right\} \right\} \quad (1)$$

where  $L$  is the sample thickness,  $l^*$  is the sample transport mean free path of scattered light,  $k_0$  is the wave factor in vacuum ( $k_0 = 2\pi/\lambda$ ),  $z_0$  is the distance that the light must travel through the sample before becoming randomized,  $z_0 = l^*$ . The only unknown parameter ( $L/l^*$ ) was obtained for each sample by comparison with the previously determined value of  $L/l^*$  and the intensity of the diffused wave for pure water ( $L/l^*(\text{H}_2\text{O}) = 26.3$ ,  $I_{\text{H}_2\text{O}} = 31.8$  kHz). The general tendency for the performed experiments is that the values of  $L/l^*$  decrease as the concentration of sodium alginate is increased with values between 30 and 12.

From the MSD of the spherical probes of known radius ( $R = 250$  nm) the frequency dependence of the complex shear modulus can be obtained from the generalized Stokes–Einstein equation:

$$\tilde{G}(s) = \frac{k_B T}{\pi R s \langle \Delta \tilde{r}^2(s) \rangle} \quad (2)$$

where  $\tilde{G}(s)$  is the viscoelastic spectrum as a function of Laplace frequency  $s$  (tilde denotes the unilateral Laplace transform),  $k_B$  is the Boltzmann constant,  $R$  is the radius of the spherical probes,  $T$  is the absolute temperature and  $\langle \Delta \tilde{r}^2(s) \rangle$  is the Laplace transform of the mean square displacement  $\langle \Delta r^2(t) \rangle$ . This equation can be expressed in the Fourier frequency domain:

$$G^*(\omega) = \frac{k_B T}{\pi R i \omega \mathcal{F} \langle r^2(t) \rangle} \quad (3)$$

where  $\mathcal{F} \langle r^2(t) \rangle$  is the Fourier transform of the mean square displacement. Assuming a local power law form for the mean square displacement, we can express  $G^*(\omega)$  as a function of the experimentally measured MSD  $\langle \Delta r^2(t) \rangle$ :

$$G^*(\omega) = \frac{k_B T}{\pi R \langle \Delta r^2(1/\omega) \rangle \Gamma[1 + \alpha(\omega)]} \quad (4)$$

$$G'(\omega) = G^*(\omega) \cos \left[ \frac{\pi \alpha(\omega)}{2} \right] \quad (5)$$

$$G''(\omega) = G^*(\omega) \sin \left[ \frac{\pi \alpha(\omega)}{2} \right] \quad (6)$$

where  $t = 1/\omega$ ,  $\alpha(t) = \partial[\ln \langle \Delta r^2(t) \rangle] / \partial[\ln t]$  is the slope of the graph of  $\langle \Delta r^2(t) \rangle$  plotted as a function of the time in logarithmic scales evaluated at  $t$ .  $\Gamma$  is the gamma function which serves as conversion factor of the transform.

With this setup at the experimental conditions written above,  $G'$  and  $G''$  of aqueous solutions of sodium alginate in the semi-dilute entangled and concentrated regimes (2, 4, 8, 14, 20, 24 and 32 g L<sup>-1</sup>) can be measured in the range between 1 to 10<sup>5</sup> Hz with a good precision in addition to macrorheological measurements.

#### 2.4. DLS-based microrheology

Dynamic light scattering measurements were performed with an ALV CGS-3 goniometry system equipped with a cuvette rotation/translation unit (CRTU) and a He–Ne laser (22 mW at  $\lambda = 632.8$  nm). The system measures the time-averaged autocorrelation function of the scattered light intensity at a scattering vector defined as  $q = 4\pi n/\lambda \sin(\theta/2)$ , where  $n$  is the refractive index of the solution and  $\theta$  the scattering angle. Sodium alginate solutions for DLS measurements were prepared in test tubes (diameter  $D = 10$  mm). Filtered mother solution of sodium alginate was mixed with filtered pure water and an appropriate quantity of spherical microparticles of polystyrene ( $\varnothing = 500$  nm) covered with alkyl-OH surface. Syringe filters of 0.80  $\mu\text{m}$  and 0.2  $\mu\text{m}$  were used for aqueous solutions of sodium alginate and pure water respectively. The analyzed concentrations of sodium alginate were 1, 2, 4 and 7.7 g L<sup>-1</sup> at a fixed temperature of 25 °C. The concentration of microparticles was fixed to 0.005% w/w, high enough to obtain a much higher scattered intensity in comparison with the scattered intensity coming from the polymer chains but low enough to avoid multi-scattering. This concentration of microparticles was experimentally determined considering the relation of the scattered intensity for microparticle aqueous dispersion ( $I_{\text{mp}}$ ) and aqueous solution of sodium alginate for a concentration of 8 g L<sup>-1</sup> ( $I_{\text{alg}}$ ), obtaining a value  $I_{\text{mp}}/I_{\text{alg}} = 30$  for the chosen concentration of microparticles.

As for DWS, the obtained intensity autocorrelation function  $g^{(2)}(t)$  was converted into the field autocorrelation function  $g^{(1)}(t)$  by the Siegert relation ( $\beta = 1$ ),  $g^{(2)}(t) = 1 + [g^{(1)}(t)]^2$ , the mean square displacement (MSD =  $\langle \Delta r^2(t) \rangle$ ) was then calculated by the following equation valid for low concentrated aqueous solutions of sodium alginate:

$$g^{(1)}(q, t) = \exp \left[ -\frac{\langle \Delta r^2(t) \rangle \cdot q^2}{6} \right] \quad (7)$$

#### 2.5. Brillouin light scattering (BLS)

The longitudinal sound velocity  $V_L$  has been measured locally in aqueous solutions of sodium alginate in the semi-dilute entangled and concentrated regimes (4, 8, 14, 20, 24 and 32 g L<sup>-1</sup>) by the Brillouin light scattering (BLS) technique in the backscattering geometry (see insert in Fig. 1). The experimental setup was



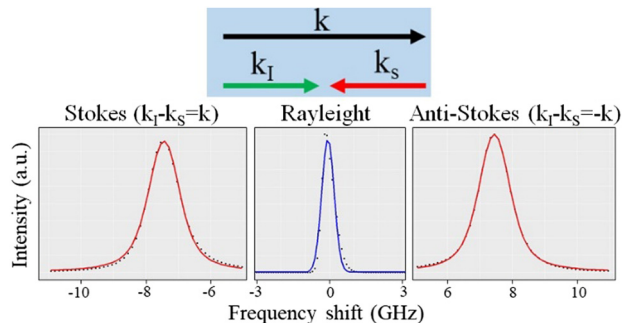


Fig. 1 BLS spectrum with fitting of the Stokes (left) and anti-Stokes (right) peak and of the Rayleigh peak (center) for instrumental linewidth (314 MHz). The back-scattering geometry sketched in insert shows the coupling between the light and a wave for a bulk transparent medium defined by  $(\mathbf{k}_I, \mathbf{k}_S) = 180^\circ$ .

composed mainly by an incident light of a longitudinal single mode laser at a wavelength  $\lambda_L = 532$  nm (Quantel Torus solid laser), a  $2 \times 3$ -pass tandem Fabry–Perot interferometer (Table Stable company) and a photodetector in addition to a set of optical fixtures to filter and to focalize the light.<sup>36–38</sup> The amplitude of the wave vector  $k$  of the bulk acoustic wave, which is backscattering the incoming light is defined by:

$$k = \frac{4 \cdot \pi \cdot n}{\lambda_L} \quad (8)$$

where  $n$  is the refractive index of the aqueous solutions of sodium alginate. It increases as a linear function with the concentration of polymer and is close to that of water ( $n = 1.331$ )<sup>39</sup> (for  $40 \text{ g L}^{-1}$  alginate solution  $n = 1.338$ ).

The intensity of the incident light in the polymer solution was maintained constant around 100 mW for all the measurements. The back-scattered light was recorded in the Stokes and anti-Stokes region, until a photon count of at least 1000 for the Brillouin peak. A typical BLS spectrum is shown in Fig. 1. Only a single peak is observed indicating that aqueous solutions of sodium alginate are homogeneous on the phonon wavelength scale ( $0.3 \mu\text{m}$  with  $532 \text{ nm}$  excitation).

The analysis is focused on the characteristic inelastic peaks from the sample that appear in the Stokes and anti-Stokes region with a negative and positive frequency shift. These peaks are analyzed to determine the frequency shift ( $f_B$ ) and the full width at half maximum ( $\Gamma_B$ ). Each of these two experimental peaks represent a convoluted signal as a result of the addition of the instrumental and the sample contribution. To determine the instrumental contribution, it was performed an experiment using a polished metal part collecting the high elastic scattered light by the rough surface. It was found that the elastic peak is well reproduced by a Gaussian distribution with null (0) frequency shift and a linewidth of  $\sigma_d = 314$  MHz (see Fig. 1). Thus, to obtain the characteristic linewidth of the sample, the measured peaks have to be deconvoluted into a Gaussian peak with the device linewidth ( $\sigma_d = 314$  MHz) and the peak containing the characteristic linewidth of the studied sodium alginate solution.

The most accurate fitting of this experimentally obtained peaks was achieved by a Voigt profile (eqn (9)) that is given by a

convolution of a Gaussian distribution (eqn (10)) and a Lorentz distribution (eqn (11)) with two parameters,  $\sigma$  (Gaussian linewidth) and  $\gamma$  (Lorentzian linewidth):

$$V(f; \gamma, \sigma) = \int_{-\infty}^{\infty} G(f'; \sigma) L(f - f'; \gamma) df' \quad (9)$$

$$G(f; \sigma) = \frac{1}{\sigma\sqrt{2\pi}} e^{-f^2/2\sigma^2} \quad (10)$$

$$L(f; \gamma) = \frac{\gamma/\pi}{f^2 + \gamma^2} \quad (11)$$

From the fittings of the obtained peaks for the aqueous solutions of sodium alginate at different concentrations, it was found systematically that the Gaussian linewidth of the Voigt profile ( $\sigma$ ) is always very close to the device linewidth ( $\sigma_d = 314$  MHz) simplifying the mathematical calculation by setting  $\sigma = \sigma_d = 314$  MHz and keeping as unique adjusted parameter the Lorentzian linewidth ( $\gamma$ ) that corresponds to the characteristic linewidth of the material ( $\gamma = \gamma_m$ ). The frequency shift ( $f_B$ ) was determined by the position of the peak. The experimental frequency shift ( $f_B$ ) and the full width at half maximum ( $\Gamma_B = 2 \cdot \gamma_m$ ) are then used to determine the sound velocity ( $v_L$ ) and the dynamical longitudinal viscosity  $\eta_L$  respectively according to the following equations:

$$v_L = \frac{f_B \lambda_L}{2n} \quad (12)$$

$$\eta_L = \frac{\rho \Gamma_B}{k^2} \quad (13)$$

where  $\rho$  is the mass density of the sample in  $\text{kg m}^{-3}$ . In the range of concentrations between  $5$  and  $30 \text{ g L}^{-1}$ ,  $\rho$  increases linearly with the concentration<sup>40</sup> from  $1002$  to  $1013 \text{ kg m}^{-3}$ . The longitudinal storage modulus  $M'$  and the longitudinal loss modulus  $M''$  of sodium alginate solutions can be finally determined by:

$$M' = \rho v_L^2 \quad (14)$$

$$M'' = 2\pi f_B \eta_L \quad (15)$$

## 2.6. Small-angle X-ray scattering (SAXS)

SAXS experiments were performed at the TRUSAXS ID02 beamline (ESRF, Grenoble).<sup>41</sup> An incident monochromatized X-ray beam with a wavelength  $\lambda = 0.995 \text{ \AA}$  was used. Scattered intensities were recorded on a two-dimensional CCD detector at two sample-to-detector distances  $0.75$  and  $8 \text{ m}$  covering a range of scattering vector magnitude,  $q$ , of  $0.04$ – $3.5 \text{ nm}^{-1}$ , where  $q = (4\pi/\lambda) \sin(\theta/2)$  with  $\theta$  the scattering angle. The azimuthal averages of the scattering intensities were calculated using the SAXS Utilities software. The studied samples of aqueous solution of sodium alginate at different concentrations in the semi-dilute entangled and concentrated regimes ( $4$ ,  $8$ ,  $14$ ,  $20$ ,  $24$  and  $32 \text{ g L}^{-1}$ ) in addition to a measurement of pure water were probed in a flow-through capillary cell (diameter  $\sim 2 \text{ mm}$ ) under controlled temperature ( $25 \pm 1 \text{ }^\circ\text{C}$ ). The experiments were done in quintuplicate for each concentration and





the shown results are a mean between them after the subtraction of the water background. These measurements allowed to establish the evolution of the scattered intensity as a function of sodium alginate concentration.

### 2.7. Metabolic activity assay

The mouse embryonic fibroblast cell line NIH-3T3 (from ATCC, CRL-1658) was selected to perform a metabolic activity assay since it is abundantly used in material biocompatibility testing.<sup>42,43</sup> Thus, obtained results are readily comparable to published data in the literature. The cells were cultured in DMEM (Dulbecco's Modified Eagle Medium, GIBCO) complemented with a 10% of fetal bovine serum (FBS), 1% of Glutamax supplement (GIBCO) and 1% of non-essential amino acids NEAA (GIBCO) giving the complete medium in a 5% CO<sub>2</sub> incubator at 37 °C. They were seeded on 2D monolayers in the well plate optimized for cell attachment of 96-well-plates (TPP) with an area of 0.33 cm<sup>2</sup> per well. Cells were seeded at 20 000 cells/200 μL (60 000 cells cm<sup>-2</sup>) of complete culture medium. The next day, the culture medium was removed and replaced by fresh culture medium containing or not sodium alginate.

The selected concentrations of sodium alginate solutions were 2.5, 5 and 10 g L<sup>-1</sup>, high enough to be in the concentrated regime with entangled polymer chains but low enough to have low viscosities that allow their manipulation. The samples were prepared by dissolving a mass of sodium alginate powder in the complete medium by magnetic stirring during 12 hours. The used sodium alginate powder (MP Biomedicals) was not a biological grade reagent. It can contain contaminants inducing adverse cell reactions or undesired and uncontrolled interactions with cells including endotoxins, protein contaminants, elemental impurities and microbial bioburden according to the literature.<sup>44–47</sup> To minimize the presence of these contaminants, two steps were efficiently included to prevent contamination in the culture: (1) the sodium alginate powders were sterilized by UV exposure for 20 minutes and (2) the DMEM used for the preparation of sodium alginate solutions was supplemented with a 1% of antibiotics (streptomycin and penicillin).

After 24 h of incubation, plates were washed twice with DMEM, followed by the addition of 100 μL of a 10% (v/v in culture medium) WST-1 cell proliferation reagent (Roche Diagnostic GmbH, Mannheim, Germany) for 2 h of incubation at 37 °C and 5% CO<sub>2</sub>. The absorbance was measured at 450 and 630 nm using an ELISA plate reader. Metabolic activity for each well was calculated as the difference of absorbance (*A*) at the two wavelengths (*A*<sub>450nm</sub>–*A*<sub>630nm</sub>) and the normalized metabolic activity was determined individually for each sample as the ratio between the cell metabolic activity of the sample and the mean cell metabolic activity of the negative control (unexposed cells). Experiments were repeated 3 times with independent cell cultures and including at least 6 wells per plate.

Results are presented in the form of boxplots of the cell metabolic activity normalized by the mean value of the negative control in which the data of each of the individual wells and the different plates are included. Each box (Fig. 14b) is divided by a line at the median representing the data from the low to the up quartile.

The upper and lower whiskers delimit the actual data points without considering the outliers; being the outliers the data outside 1.5 times the interquartile range (IQR – see Fig. 14b). In addition, the mean value without considering the outliers has been added in the center of the box. For statistical analysis, the experimental results were compared to their corresponding control values using an ANOVA with Dunnet's post-test to compare the result of each condition with the negative control. In all the cases a *p* value of < 0.05 was considered to be significant.

## 3. Results

Different complementary experimental methods were used to investigate the zero-shear specific viscosity ( $\eta_{sp}$ ) of sodium alginate solutions defined as  $(\eta - \eta_s)/\eta_s$  where  $\eta$  is the viscosity of the solution extrapolated at low shear rates, low frequencies or high times and  $\eta_s$  the viscosity of the solvent for each regime of concentration:

- Semi-dilute untangled regime (0.1–2 g L<sup>-1</sup>): Newtonian viscosity determined by shear rheology and by the slope of the MSD at long times determined by DLS-microrheology for the alginate concentrations 1 and 2 g L<sup>-1</sup>.

- Semi-dilute entangled regime (2–8 g L<sup>-1</sup>): (1) first Newtonian shear viscosity ( $\eta_0$ ) obtained from the fitting of steady-state flow measurements with Cross model (Table 1) and (2) slope of the MSD at long times determined by DLS-microrheology.

- Concentrated regime (8–40 g L<sup>-1</sup>): (1) first Newtonian shear viscosity ( $\eta_0$ ) of the Cross model from the fitting of the shear viscosity as function of the shear rate and (2) value of  $\eta'_0$  of the Cross model from the fitting of the dynamic viscosity ( $\eta' = 2\pi G''/\omega$ ) as function of the frequency combining oscillatory microrheology and DWS-based microrheology.

These values of the zero-shear specific viscosity are presented in Fig. 2 determined by the different methodologies obtaining a good superposition. For the lower studied concentrations, the power law exponent of the concentration dependence of the viscosity found experimentally is 0.53 very close to the theoretical value for a polyelectrolyte solution in the semi-dilute untangled regime ( $\eta \sim c^{1/2}$ ). The explanation is that all the studied concentrations are above the overlap concentration  $c^*$  that is commonly very low for polyelectrolytes due to their stiffness and electrostatic repulsive interactions between chains and monomers. In the same range of concentrations but in the presence of salt (NaCl 0.1 M), the expanded conformation of sodium alginate is partially lost, and the chains are contracted due to the screening of the electrostatic repulsion between monomers decreasing the volume occupied by a sodium alginate coil. This change is translated into a decrease of the zero-shear specific viscosity. The exponent obtained experimentally for the viscosity is 1.21 being very close to the theoretical one for polyelectrolyte semi-dilute solutions with added salt ( $\eta \sim c^{5/4}$ ).

Increasing the sodium alginate concentration, the polymer chains become closer one to the other leading to a solution in the semi-dilute entangled regime from the critical concentration ( $C_c = 2 \text{ g L}^{-1}$ ). The characteristic power law exponent



found experimentally for this regime is 1.45 also very close to the theoretical value for a polyelectrolyte ( $\eta \sim c^{3/2}$ ). Above the concentration  $C^{**} = 8 \text{ g L}^{-1}$ , the electrostatic repulsions between chains become negligible when the density of entanglements between chains are very high and the behavior of a concentrated polyelectrolyte solution can be described by the laws of a neutral polymer. The characteristic power law exponent of 3.19 found experimentally is in good agreement with the one for a neutral polymer in the concentrated regime ( $\eta \sim c^{15/4}$ ).

### 3.1. Diluted regime: determination of $M_v$

Sodium alginate chains in the diluted regime are isolated and interact only with the solvent molecules simplifying their description through the determination of the intrinsic viscosity  $[\eta]$ . The intrinsic viscosity depends on the concentration and size of the dissolved macromolecules, as well as on the solvent quality and temperature. For these conditions, the specific viscosity ( $\eta_{sp}$ ) of a solution can be described by first order polynomial models, the Huggins and Kraemer equations:

$$\frac{\eta_{sp}}{C} = [\eta] + k_H[\eta]^2 C \quad (16)$$

$$\frac{\ln(\eta_{rel})}{C} = [\eta] + k_K[\eta]^2 C \quad (17)$$

where  $C$  is the concentration of sodium alginate,  $\eta_{rel}$  is the relative viscosity ( $\eta/\eta_s$ ),  $\eta_{sp}$  is the specific viscosity.  $k_H$  and  $k_K$  are the Huggins and Kraemer coefficient respectively reflecting the quality of the solvent. Experimental results indicate that the higher the affinity between polymer and solvent,<sup>48</sup> the lower is

the  $k_H$  value. At the same time, negative values for  $k_K$  are typically an indication of good solvent and positive values indicate poor ones. But most importantly, from these models, it can be determined the intrinsic viscosity  $[\eta]$  for a sodium alginate-water system at fixed temperature by extrapolation to zero concentration. The obtained  $[\eta]$  is a measure of a solute's contribution to the viscosity and can be related to the polymer viscosity average molecular weight ( $M_v$ ) by the Mark-Houwink-Sakurada equation:

$$[\eta] = KM_v^\alpha \quad (18)$$

where the values of the Mark-Houwink-Sakurada parameters ( $\alpha$  and  $K$ ) depend on the polymer-solvent interactions and temperature. They can be found in the bibliography determined by complementary techniques such as chromatography or dynamic light scattering (DLS). In saline conditions (NaCl 0.1M)<sup>49</sup> in order to screen the charges of sodium alginate chains and to get a random coil conformation supposed in eqn (18), the values are  $\alpha = 0.963$  and  $K = 1.228 \cdot 10^{-4} \text{ dL g}^{-1}$ .

The results are presented in Fig. 3 to show the determination of the intrinsic viscosity  $[\eta]$  as well as the constants  $k_H$  and  $k_K$  from the experimental data. Then, the value of  $M_v = 1 \times 10^5 \text{ g mol}^{-1}$  was determined using the Mark-Houwink-Sakurada equation (eqn (18)) being in the classical range of molecular weights found in the literature ( $5 \cdot 10^3 - 3 \cdot 10^6 \text{ g mol}^{-1}$ ).<sup>50</sup> It can be then deduced the overlap concentration  $c^*$  separating the dilute and semi-dilute unentangled regime ( $c^* = 1.45/[\eta] = 1.8 \text{ g L}^{-1}$  with  $[\eta]$  close to  $0.8 \text{ L g}^{-1}$  (see Fig. 3). This value is deduced from  $[\eta]$  determined from shear viscosity measurements of aqueous solutions of sodium alginate with NaCl as explained above. It cannot be

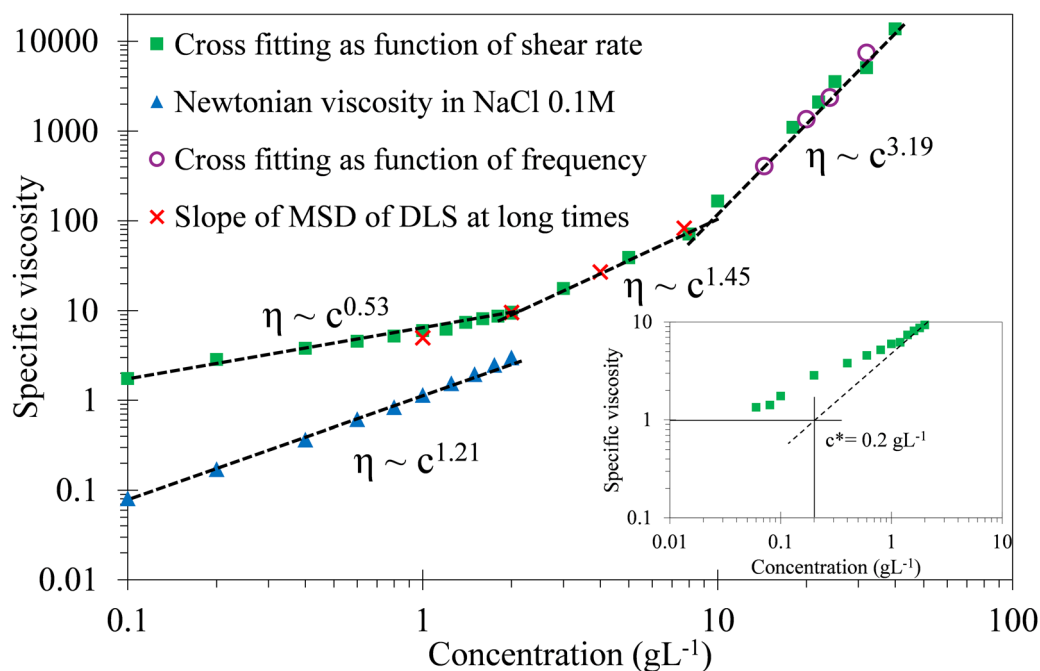


Fig. 2 Specific viscosity as a function of the alginate concentration for sodium alginate solutions obtained by shear rheology, DWS and DLS. The plot for the determination of the overlap concentration  $c^*$  is shown in the insert.



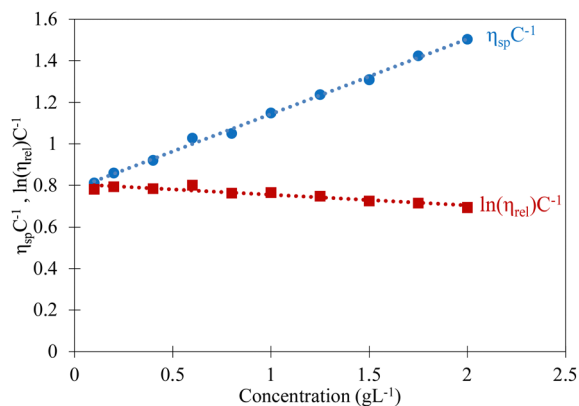


Fig. 3 Representation to determine the intrinsic viscosity of sodium alginate based on Huggins and Kraemer equations from the y-axis-intercept of the linear fittings.

determined experimentally in pure water due to its very low value. In this case A. Dodero<sup>51</sup> *et al.* proposed to estimate  $c^*$  by extrapolation of the straight line to  $\eta_{sp} = 1$  to the semi-dilute untangled regime. The obtained value (see insert of Fig. 2)  $c^* = 0.2 \text{ g L}^{-1}$  is indeed much lower than the one deduced from  $[\eta]$  but very close to the value determined experimentally previously in similar sodium alginate solution.<sup>52</sup>

The obtained values of  $k_H$  close to 0.5 and  $k_K$  close to 0 suggest a polymer-solvent system close to theta-conditions.

### 3.2. Dependence of viscosity on shear rate and frequency

The results of the shear rate dependence of the viscosity of sodium alginate aqueous solutions are presented in Fig. 4 for a set of representative concentrations. The shear-thinning behavior can be explained by the disentanglement and alignment of alginate chains in the direction of the applied shear rate.

Among the different phenomenological models of shear-thinning behavior, the Cross equation (eqn (19)) was found to best fit the experimental data with the parameters summarized

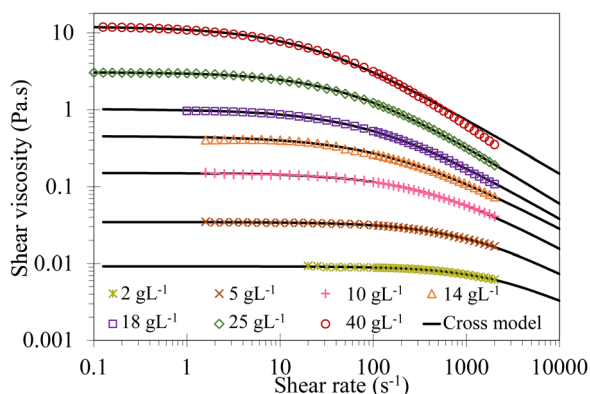


Fig. 4 Evolution of the stationary shear viscosity as function of the shear rate for aqueous solution of sodium alginate at different concentrations in the semi-dilute and concentrated regimes. The solid lines correspond to the fitting of experimental data by Cross model (eqn (19)).

Table 1 Parameters of Cross model fitting (eqn (19)) of the flow curves (Fig. 4)

$C_{\text{alg}}$ (g L <sup>-1</sup> )	$\eta_0$ (Pa.s)	$m$	$\tau_c$ (s)
2	0.009	0.19	$3.10^{-4}$
3	0.016	0.27	$4.10^{-4}$
5	0.035	0.24	$6.10^{-4}$
8	0.063	0.20	$8.10^{-4}$
10	0.15	0.23	0.002
14	0.4	0.29	0.004
18	0.97	0.26	0.009
22	1.85	0.29	0.013
25	3.14	0.25	0.019
32	4.45	0.25	0.021
40	12.06	0.28	0.045

in Table 1:

$$\eta_a = \eta_\infty + \frac{\eta_0 - \eta_\infty}{1 + \left(\frac{\dot{\gamma}}{\dot{\gamma}_c}\right)^{1-m}} \quad (19)$$

where  $\eta_0$  and  $\eta_\infty$  are limiting viscosities at zero and infinite shear rates respectively. The parameter  $m$  is a rate constant characteristic of the flow behavior in the shear-thinning region.  $\dot{\gamma}_c$  is the critical shear rate from which the shear-thinning behavior begins. The inverse of  $\dot{\gamma}_c$  can be defined as the longest relaxation time ( $\tau_c$ ) associated with the disentanglement of chains. The infinite shear rate viscosity  $\eta_\infty$  was not obtained experimentally. It was fixed to  $0.89 \cdot 10^{-3} \text{ Pa s}$  corresponding to the viscosity of water at  $25^\circ \text{C}$ . An important increase of the apparent viscosity, at low shear rates in comparison to the solvent viscosity ( $0.89 \text{ mPa s}$ ) is observed as expected for the semi-dilute entangled and concentrated regimes, showing a shear-thinning behavior. This situation confirms the big volume occupied by each sodium alginate chain and the strong inter-chain interactions responsible of the shear-thinning behavior.

The values of  $\eta_0$  are used in Fig. 2. The values of  $m$  are very similar than the ones found by Rodríguez-Rivero *et al.*<sup>29</sup> in alginate salt free solutions with nearly constant values in our case. The concentration dependence of the longest relaxation time (Fig. 5) shows two regimes<sup>53</sup> clearly differentiated by the same critical concentration of  $8 \text{ g L}^{-1}$  found with the concentration dependence of the zero-shear specific viscosity (Fig. 2). At high concentrations, the value of the exponent (2.37) is in a very good agreement with the experimental one found by other authors<sup>29</sup> and the theoretical one (7/3) expected for entangled neutral polymers in theta solvent.

Moreover, the frequency ( $10^{-2}$ – $10^5 \text{ Hz}$ ) dependence of the dynamic viscosity ( $\eta'$ ) of sodium alginate solutions in the concentrated regime was studied by combination of DWS microrheology and oscillatory macrorheology (Fig. 6a). The results of the fittings with the Cross model (eqn (19)) changing the shear rate by the frequency are summarized in Table 2. In addition, the longitudinal viscous modulus ( $M''$ ) has been obtained from BLS as described previously (eqn (15)) from the width of the Brillouin peak for very high frequency ( $\sim \text{GHz}$ ). The observed experimental linear concentration-dependence of  $M''$  (Fig. 7a) with an increase of 21% can be described by the addition of the contribution of water and the one of sodium alginate polymer by using a mixing law:<sup>54</sup>



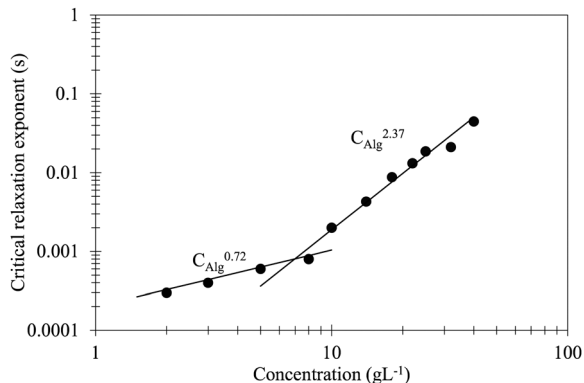


Fig. 5 Concentration-dependence of the critical relaxation time ( $\tau_c$ ) obtained from the fitting to Cross model of experimental data (Fig. 4) for aqueous solutions of sodium alginate.

$$M'' = M''_{\text{water}} \cdot x_w + M''_{\text{alginate}} \cdot (1 - x_w) \quad (20)$$

where  $x_w$  is the weight fraction of water and  $M''_{\text{water}}$  and  $M''_{\text{alginate}}$  are the intrinsic longitudinal loss modulus of water and sodium alginate, respectively.

A Brillouin experiment with pure water leads to the value  $M''_{\text{water}} = 0.0325$  GPa. We can then deduce the intrinsic longitudinal loss modulus of sodium alginate with the slope in Fig. 7a obtaining  $M''_{\text{alginate}} = 0.329$  GPa.

The value of the dynamical longitudinal viscosity ( $\eta_L$ ) can be used to evaluate the average relaxation time  $\tau$  which can be compared to the one of pure water in order to emphasize possible changes in the water dynamics induced by sodium alginate chains. An average relaxation time can be deduced according to the following equation:<sup>55</sup>

$$\langle \tau \rangle = \frac{b - b_\infty}{\Delta_c} \quad (21)$$

where  $b_\infty$  accounts for contributions to viscosity that are very fast (instantaneous) relative to the picosecond time scale investigated by BLS,  $\Delta_c$  is the relaxation strength at each sodium alginate concentration, given by relaxed ( $c_0$ ) and un-relaxed

Table 2 Parameters of Cross model fitting of the experimental evolution of  $\eta'$  as function of the frequency obtained by combined results of oscillatory macrorheology and DWS microrheology (Fig. 6a)

$C_{\text{alg}} \text{ (g L}^{-1}\text{)}$	$\eta'_0 \text{ (Pa.s)}$	$m$	$1/f_c \text{ (s)}$
14	0.36	0.16	0.016
20	1.21	0.15	0.058
24	2.10	0.18	0.085
32	6.60	0.27	0.377

( $c_\infty$ ) sound velocities ( $\Delta_c = c_\infty^2 - c_0^2$ ) and  $b = \eta_L/\rho$  is the kinematic viscosity in  $\text{m}^2 \text{s}^{-1}$  obtained from the full width at half maximum ( $\Gamma_B$ ) of the Brillouin peak. A first estimation of the relation between  $\tau$  et  $\eta_L$  can be performed if the values of  $b_\infty$  and  $c_\infty$  are here fixed to those obtained by X-ray scattering in pure water<sup>56</sup> ( $b_\infty = 2.99 \cdot 10^{-7} \text{ m}^2 \text{ s}^{-1}$  and  $c_\infty = 2860 \text{ m s}^{-1}$ ).

The increase of the relaxation time as function of the concentration of sodium alginate (Fig. 8) is related with a change of the characteristic times of molecular relaxations. The increase is more pronounced in the semi-dilute regime ( $c < c^{**} = 8 \text{ g L}^{-1}$ ) than in the concentrated regime ( $c > c^{**}$ ). This can be explained by the presence of water with different relaxation times, free and hydration water. Thus, the averaged relaxation time increases rapidly with the concentration in the semi-diluted regime due to an increase of the fraction of hydration water. However, this increase slows down in the concentrated regime probably due to an increase of polymer–polymer rather than polymer–water interactions.

A more rigorous analysis can be performed considering a two-step relaxation associated with hydration and bulk water with characteristic times,  $\tau_h$  and  $\tau_b$ , respectively leading to the following equation:<sup>54</sup>

$$\frac{\Delta_0 b - b_0}{\Delta_c b - b_\infty} - 1 = N_h (1 - \varepsilon) f_r \quad (22)$$

where  $\Delta_0$  and  $b_0$  are respectively the relaxation strength and the kinematic viscosity of pure water,  $\varepsilon$  is the relative fraction of hydration and bulk water,  $f_r$  is the fraction of polymer-to-water molecules and  $N_h$  is the solvation number (the average number

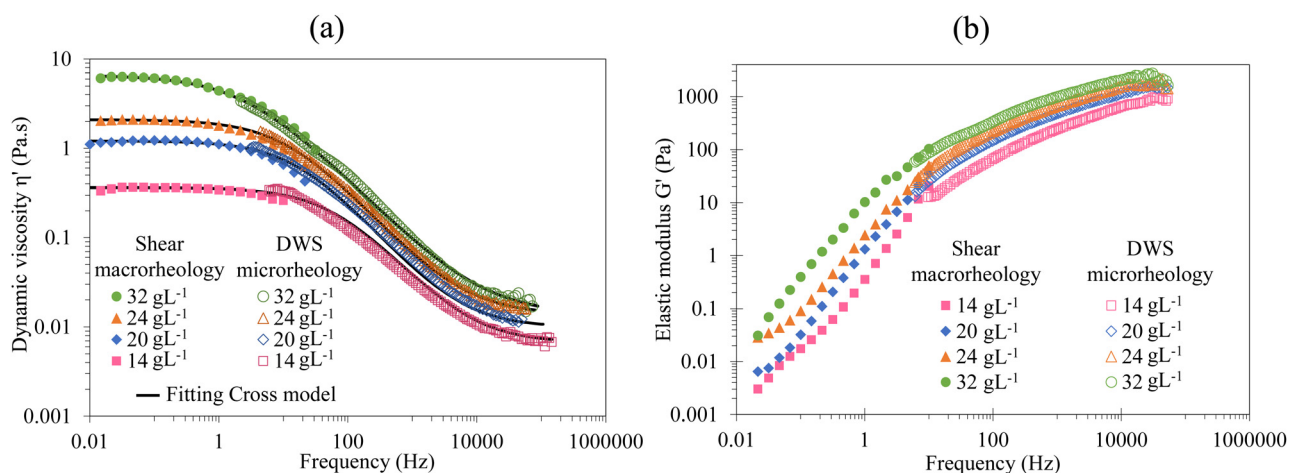


Fig. 6 Evolution of (a) the dynamic viscosity  $\eta'$  and (b) elastic modulus as function of the frequency at 25 °C for different sodium alginate concentrations (14, 20, 24 and 32  $\text{g L}^{-1}$ ) combining shear macrorheology and diffusing-wave spectroscopy.





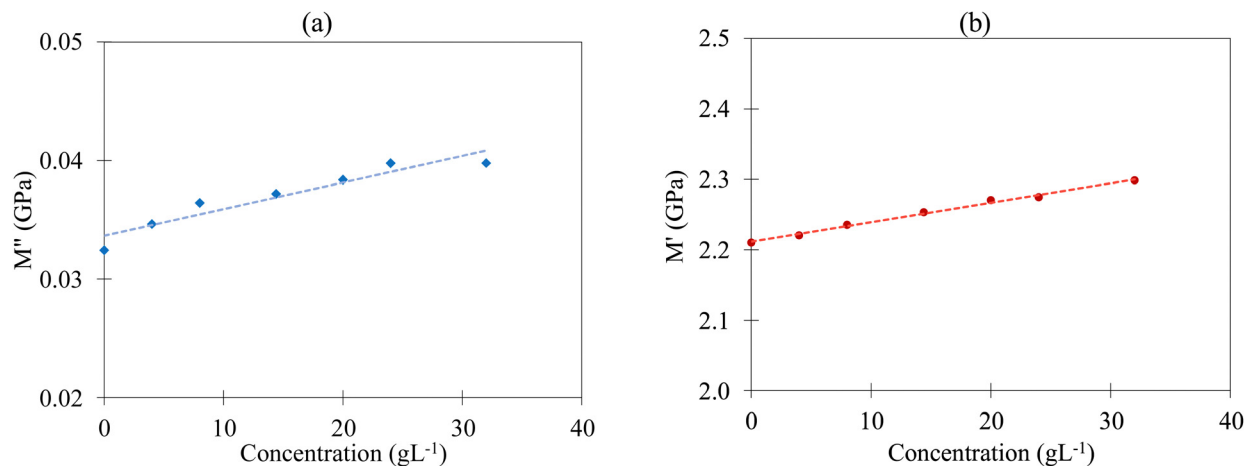


Fig. 7 Evolution of the (a) longitudinal loss modulus  $M''$  and (b) longitudinal elastic modulus  $M'$  of aqueous solutions of sodium alginate as function of the concentration at high frequencies ( $\sim$ GHz) determined by BLS.

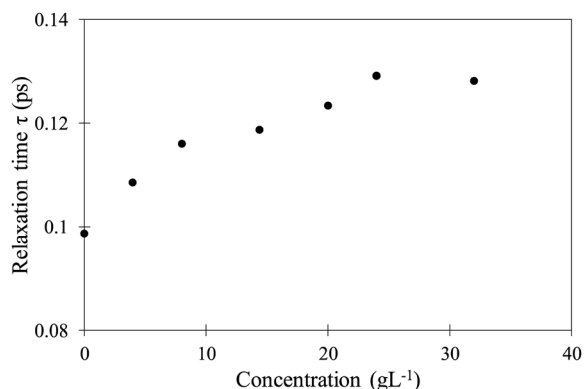


Fig. 8 Concentration-dependence of the critical relaxation time obtained from the longitudinal loss moduli (FWHM of the Brillouin spectra).

of molecules bound to the compound more strongly they are bound to other water molecules).

The prediction of eqn (22) is evaluated in Fig. 9. A linear dependence of  $[(\Delta_0 b - b_0)/(\Delta_c b - b_\infty)]^{-1}$  as function of the polymer-to-water molar fraction is observed. The slope gives a

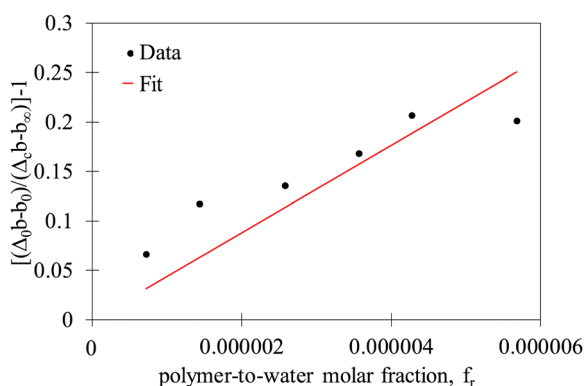


Fig. 9 Linearized model plot of eqn (22) (circles) and linear fit (red line) giving a gradient  $N_h(\varepsilon - 1) = 44\,000$ .

value of  $N_h \cdot (1 - \varepsilon) = 44000 \pm 4000$ . This value is considerably higher than the value found for gelatin by Bailey *et al.*<sup>54</sup> This can be explained by a stronger polyelectrolyte behavior of sodium alginate than gelatin. The stronger repulsions between the chains and the stronger hydrophilicity of sodium alginate leads to higher solvation numbers.

### 3.3. Dependence of elasticity on frequency

Aqueous solutions of sodium alginate begin to show a relevant elasticity in the concentrated regime when the density of entanglements increases and the distance between them decreases. The combination of macro and microrheology (DWS) allows a continuous study of the shear elastic modulus between  $10^{-2}$ – $10^5$  Hz finding a good agreement for intermediate frequencies as shown in Fig. 6b for aqueous solutions of sodium alginate of 14, 20, 24 and 32  $\text{g L}^{-1}$ .

In addition, the longitudinal elastic modulus ( $M'$ ) has been obtained from BLS (eqn (14)) from the frequency shift of the Brillouin peak at very high frequency ( $\sim$ GHz). The observed experimental linear concentration dependence of  $M'$  (Fig. 7b) with an increase of 4% can be described as previously:

$$M' = M'_{\text{water}} \cdot x_w + M'_{\text{alginate}} \cdot (1 - x_w) \quad (23)$$

where  $x_w$  is the weight fraction of water and  $M'_{\text{water}}$  and  $M'_{\text{alginate}}$  are the intrinsic longitudinal elastic modulus of water and sodium alginate, respectively.

A BLS experiment with pure water leads to the value  $M'_{\text{water}} = 2.21$  GPa. We can then deduce the intrinsic longitudinal elastic modulus of sodium alginate with the slope in Fig. 7b obtaining  $M'_{\text{alginate}} = 4.98$  Pa. It should be noted that the increase of  $M'$  (4%) is lower than the one of  $M''$  (21%). The addition of polymer has a stronger effect on the width of the Brillouin peak and then microscopic viscosity of the aqueous solution of sodium alginate than on frequency shift of the Brillouin peak with a high modulus of water (2.21 Pa) and small effect of polymer.



### 3.4. Structure

**3.4.1. Determination of the persistence length ( $L_p$ ).** The determination of the viscoelastic properties of aqueous solutions of sodium alginate in a wide range of frequencies between  $10^{-2}$  and  $10^5$  Hz opens the possibility to determine the persistence length ( $L_p$ ) of sodium alginate chains based on the frequency-dependence of the complex modulus ( $G^* \sim \omega^\delta$ ). For solutions in the concentrated regime, at low frequencies, the complex modulus ( $G^*$ ) follows a power law dependence with an exponent  $\delta = 5/9$  (Zimm–Rouse mode). Then at higher frequencies, the length scale decreases and the chain rigidity starts to control the viscoelasticity with an exponent of  $\delta = 3/4$  (bending mode). The persistence length of the polymer can be then determined from the critical frequency ( $\omega_c$ ) at the transition between the Zimm–Rouse and bending mode by application of the following equation:<sup>57</sup>

$$\omega_c = \frac{k_B T}{8\eta_s L_p^3} \quad (24)$$

where  $k_B T$  is the thermal energy of the system and  $\eta_s$  the viscosity of the solvent (0.89 mPa s for water at 25 °C).

In order to determine  $\omega_c$ , the data were fitted with power law equations as shown as example in Fig. 10 for an aqueous solution of sodium alginate with a concentration of 8 g L<sup>-1</sup>. The values of  $L_p$  for the different concentrations of sodium alginate are collected in the Table 3. The value of the  $\omega_c$  increases with the concentration while the value of  $L_p$  decreases. For higher alginate concentrations the critical frequency is too high to be accurately determined.

To evaluate theoretically the values of  $L_p$  and the concentration dependence, it is necessary to consider the electrostatic effects of the persistence length. We can use the Odjik Skolnick Fixman (OSF) relations:

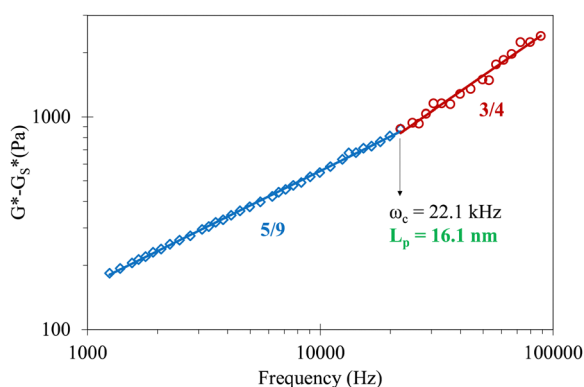


Fig. 10 Determination of the critical frequency ( $\omega_c$ ) for an aqueous solution of sodium alginate with a concentration of 8 g L<sup>-1</sup>.

Table 3 Persistence length ( $L_p$ ) of sodium alginate chains for aqueous solutions at different concentrations

Concentration (g L <sup>-1</sup> )	$\omega_c$ (kHz)	$t_c$ (ms)	$L_p$ (nm)
2	9.9	0.10	21.0
4	14.2	0.070	18.6
8	22.1	0.045	16.1
14	30.6	0.033	14.4

$$L_p = L_{p,e} + L_{p,0} \quad (25)$$

$$L_{p,e} = \frac{(l_B/d)^2}{4l_b} \kappa^{-2} \quad (26)$$

$$\kappa^{-1} = \frac{1}{\sqrt{4\pi l_B C_f}} \quad (27)$$

where  $L_{p,e}$  and  $L_{p,0}$  are the electrostatic and intrinsic contributions to  $L_p$  respectively,  $l_B$  is the Bjerrum length (0.71 nm in water),  $\kappa^{-1}$  is the Debye–Hückel screening length,  $d$  is the distance between charges on alginate chains ( $d = 0.5 \text{ nm}^{58}$ ) and  $C_f$  is the ionic concentration of the solution. This model considers that the electrostatic charges along the chain tend to increase the local rigidity of the sodium alginate. For the present case, even if solutions were always prepared in pure water without addition of any salt, the counterions ( $\text{Na}^+$ ) can have an important effect on the ionic strength of the medium and then on the local rigidity. Thus, higher alginate concentrations imply higher  $\text{Na}^+$  concentrations, screening the electrostatic repulsion and therefore decreasing the electrostatic contribution to the persistence length ( $L_{p,e}$ ). Zhang *et al.* reported the value of  $L_{p,0}$  (12.5 nm),<sup>59</sup> and with this value we calculate the persistence length as a function of alginate concentration and compare it with our experimental value (Fig. 11). Our experimental result is reasonably close to the calculated values. We can see that the electrostatic effect is screened at the concentrations studied (above 2 g L<sup>-1</sup>) and the persistence length is close to  $L_{p,0}$ .

**3.4.2. Small-angle X-ray Scattering (SAXS).** The scattered intensity is plotted as a function of the scattering vector  $q$  in Fig. 12 for the different concentrations of sodium alginate. The scattering properties of neutral polymer solutions can be described by an Ornstein–Zernike function from which the average spatial extent of random thermal fluctuation or the correlation length  $\zeta$  can be deduced. In the case of polymer chains with rigid or semi-rigid segments coming from electrostatic repulsions of polyelectrolyte chains as example, a second length is required to account for finite cross-sectional area of chains. Moreover molecular associations are the origin of

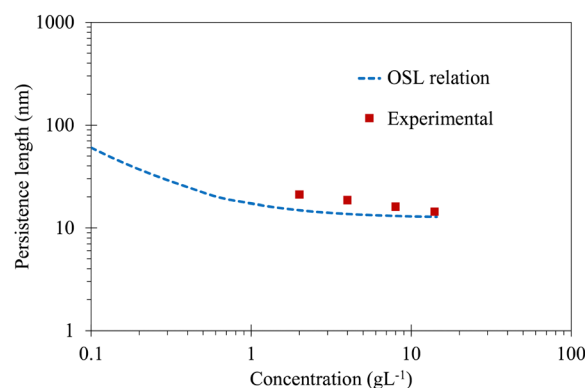


Fig. 11 Variation of the persistence length measured and calculated from OSF theory (eqn (25) and (26)) as a function of the concentration of sodium alginate.



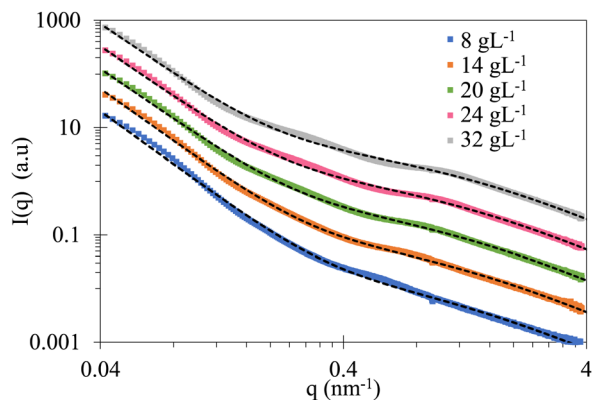


Fig. 12 Scattering intensity as a function of the modulus of scattering vector  $q$  of the SAXS study on sodium alginate solutions at different concentrations (8–32 g L<sup>-1</sup>). The data at the different concentrations are displaced vertically by a factor  $3^n$  ( $n = 1, 2, 3, 4, 5$ ) for a better visualization of the data. Dashed lines correspond to the fitting with eqn (5) of F. Horkay *et al.*<sup>60</sup>

scattering contribution at small  $q$  as observed in Fig. 12. The total scattering curve can be then defined in terms of these three different contributions as proposed by Horkay *et al.*<sup>60</sup> The very good fitting of our experimental data (dashed lines in Fig. 12) allows us to determine the correlation length  $\xi$ . Its concentration dependence is well described by a power law (Fig. 13) with an exponent (0.55) very close to the experimental one found by other authors in sodium alginate<sup>61</sup> and the theoretical value predicted for polyelectrolyte solution.<sup>62</sup>

### 3.5. Metabolic activity assay

Sodium alginate is widely considered as a biocompatible material if it is purified appropriately.<sup>63</sup> The biocompatibility of a material is defined as the material property, which, after implantation in a living organism, does not produce adverse reactions and is accepted by the adjacent tissue.<sup>64</sup> Even if no *in vivo* studies are performed, a classical assumption is that an *in vitro* normalized cell viability value higher than 0.8 indicates good biocompatibility.<sup>65</sup> The biocompatibility of the sodium alginate was assessed using the WST-1 assay. This assay reports

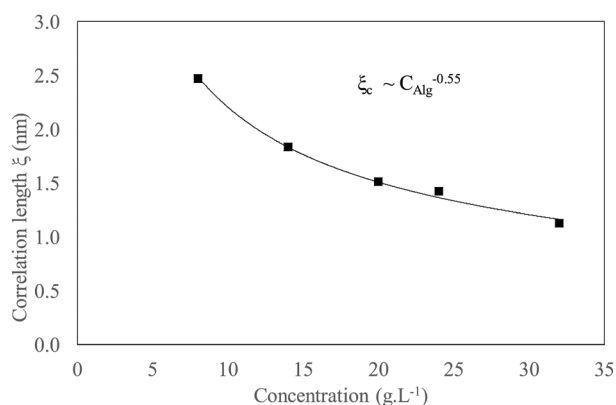


Fig. 13 Concentration-dependence of the correlation length ( $\xi$ ) of the sodium alginate solutions determined by SAXS.

the metabolic activity of the cells as it is based on the cleavage of the tetrazolium salt WST-1 to formazan by cellular mitochondrial dehydrogenases. Even if sodium alginate is used commonly in hydrogel form for biomedical applications, there are numerous parameters of a biomedical device that can affect the cell metabolic activity. Some of them occur at the molecular level. They are thus related with the physicochemical nature of the sodium alginate chains, hence the interest in evaluating the biocompatibility of the aqueous solutions of sodium alginate. In addition, this study will serve to assess the steps included in the methodology of elaboration of samples to prevent the contamination of the sodium alginate reagent. Normalized results are presented in Fig. 14a in the form of boxplots of the metabolic viability normalized by the mean value of the negative control in which the data of each of the individual wells and the different plates are included.

There is no significant decrease of metabolic activity of fibroblasts whatever the sodium alginate concentration used. Thus, the studied alginate solutions can be considered biocompatible in the range of studied concentrations. However, we observed at the lower concentration (2.5 g L<sup>-1</sup>) a statistically significant increase of the viability. This increase of viability at low concentration followed by a decrease at high concentration could be ascribed to the increase of viscosity as function of the sodium alginate concentration. For example, when the concentration of sodium alginate is increased from 5 to 10 g L<sup>-1</sup>, the viscosity is increased from 35 to 147 mPa s. The decrease in metabolic activity with increasing viscosity could be related to differential diffusion kinetics of gases and nutrients and metabolic waste. Another explanation mentioned in the literature could be the role of proteins and polyphenolic compounds that frequently contaminate sodium alginate reagents.<sup>63</sup>

## 4. Conclusions

The elaboration and complete investigation of sodium alginate aqueous solutions leads to a comprehensive study from molecular to macroscopic scale. Firstly, a rheological study was performed finding three regimes of concentration. A polyelectrolyte behavior was identified at low concentrations in the semi-dilute unentangled regime with strong repulsion between negatively charged carboxylate groups. These electrostatic interactions were screened by the addition of salt in order to determine the intrinsic viscosity and the viscosity average molecular weight. The parameters of the Huggins and Kraemer plot have confirmed a polymer-solvent system in theta-conditions. The polyelectrolyte behavior remains in the semi-dilute entangled regime until a concentration around 8 g L<sup>-1</sup>. At high concentrations the viscosity scales according to a neutral polymer behavior since the electrostatic repulsions become negligible in comparison to the effect of the entanglements. The viscosity was studied as a function of the shear rate and the frequency by a combination of shear macrorheology and diffusive-wave spectroscopy (DWS). The combined results obtained over seven frequency decades (10<sup>-2</sup>–10<sup>5</sup> Hz) show a



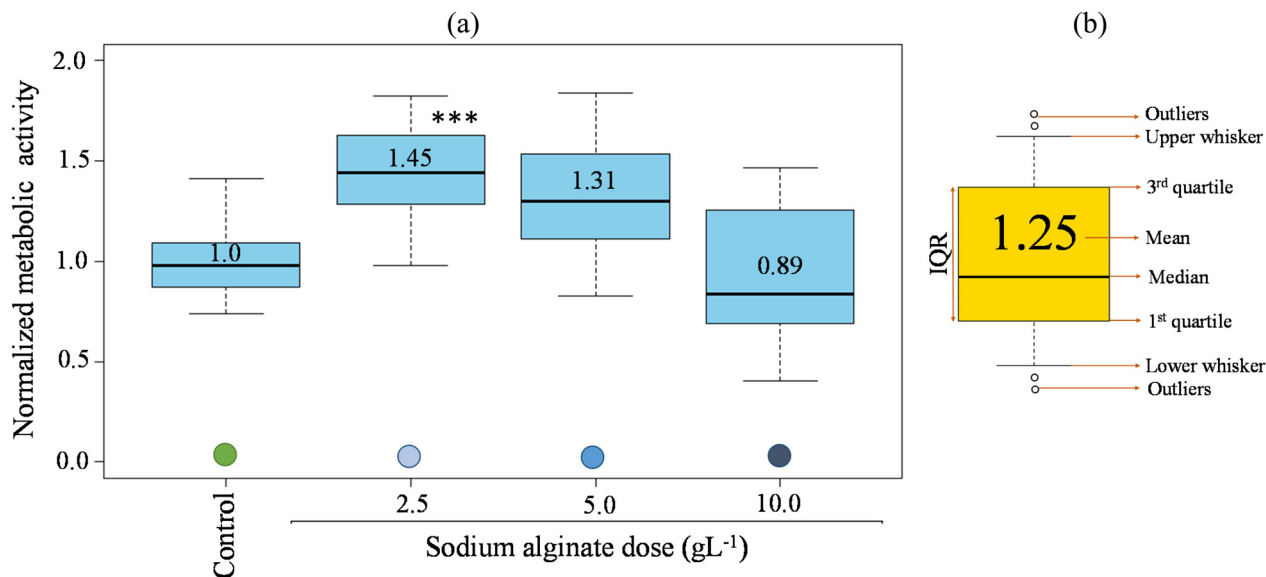


Fig. 14 (a) Normalized metabolic activity of fibroblasts exposed to sodium alginate solutions at different concentrations after 24 h of exposure (6 wells for each condition and 3 biological replicates). Significance indicated by \* =  $p < 0.05$ , \*\* =  $p < 0.005$  and \*\*\* =  $p < 0.0001$ , when sample treatments are compared by Dunnet's test to the control. (b) Interpretation of the boxplot for the metabolic activity representation. The absence of symbol (\*) means no statistically significant difference with the control.

very good concordance. The shear rate and frequency dependence of the viscosity were successfully fitted with the Cross model for shear thinning fluids and related with the entanglement/disentanglement of the polymer chains. The persistence length of the alginate chains was determined as function of the concentration from the measurements of DWS by identification of the characteristic frequency corresponding with the transition between a behavior following Zimm-Rouse and bending mode. The longitudinal viscosity and the longitudinal elastic modulus at very high frequencies ( $\sim$ GHz) determined from the spectra obtained by Brillouin light scattering were found to be many orders of magnitude higher than the moduli determined by low frequency ( $10^{-2}$ – $10^2$  Hz) rotational rheology. Complementary small-angle X-ray scattering (SAXS) experiments were also performed to directly probe the structural properties. The evolution of the scattered intensity as function of the scattering wave vector modulus  $q$  was described by an expression taking into account random thermal concentration fluctuations, finite cross-sectional area of polymer chains and large molecular associations at small  $q$ . The exponent of the power law concentration dependence of the correlation length is close to the one predicted for polyelectrolyte solutions. As conclusion of all this investigation, the entangled network of the sodium alginate solution was described by the determination of their characteristic sizes as function of the concentration (correlation length and persistence length). Moreover, the biocompatibility of sodium alginate in the studied range of concentrations (2.5–10 g L<sup>-1</sup>) was confirmed by metabolic activity assays using mouse embryonic fibroblasts indicating future biomedical applications.

## Conflicts of interest

There are no conflicts to declare.

## Acknowledgements

“ANR (Agence Nationale de la Recherche) and CGI (Commissariat à l'Investissement d'Avenir) are gratefully acknowledged for their financial support of this work through Labex SEAM (Science and Engineering for Advanced Materials and devices), ANR-10-LABX-0096 and ANR-18-IDEX-0001”. ESRF is also acknowledged for provision of synchrotron beamtime (in-housse beam-time). LRP is part of Institut Carnot PolyNat (Investissements d'Avenir – grant agreement #ANR-16-CARN-0025-01), LabEx Tec21 (Investissements d'Avenir – grant agreement no. ANR-11-LABX-0030) and Glyco@Alps programme (Investissements d'Avenir – grant agreement #ANR-15-IDEX-02).

## Notes and references

- M. Abhilash and D. Thomas, in *Biopolymer Composites in Electronics*, ed. K. K. Sadasivuni, D. Ponnamma, J. Kim, J.-J. Cabibihan and M. A. ALMaadeed, Elsevier, 2017, 405–435.
- A. Haug, B. Larsen and O. Smidsrod, *Acta Chem. Scand.*, 1967, **21**, 691–704.
- K. I. Draget and C. Taylor, *Food Hydrocolloids*, 2011, **25**, 251–256.
- K. Y. Lee and D. J. Mooney, *Prog. Polym. Sci.*, 2012, **37**, 106–126.
- R. Abka-khajouei, L. Tounsi, N. Shahabi, A. K. Patel, S. Abdelkafi and P. Michaud, *Mar. Drugs*, 2022, **20**, 364.
- H. Hecht and S. Srebnik, *Biomacromolecules*, 2016, **17**, 2160–2167.
- I. Braccini, R. P. Grasso and S. Perez, *Carbohydr. Res.*, 1999, **317**, 119–130.
- T. E. Jørgensen, M. Sletmoen, K. I. Draget and B. T. Stokke, *Biomacromolecules*, 2007, **8**, 2388–2397.





- 9 O. Aarstad, E. B. Heggset, I. S. Pedersen, S. H. Bjørnøy, K. Syverud and B. L. Strand, *Polymers*, 2017, **9**, 378.
- 10 A. Jork, F. Thürmer, H. Cramer, G. Zimmermann, P. Gessner, K. Hämel, G. Hofmann, B. Kuttler, H.-J. Hahn, O. Josimovic-Alasevic, K.-G. Fritsch and U. Zimmermann, *Appl. Microbiol. Biotechnol.*, 2000, **53**, 224–229.
- 11 S. K. Tam, J. Dusseault, S. Bilodeau, G. Langlois, J.-P. Hallé and L. Yahia, *J. Biomed. Mater. Res., Part A*, 2011, **98A**, 40–52.
- 12 S. Sugiono, M. Masruri, T. Estiasih and S. B. Widjarnako, *J. Aquat. Food Prod. Technol.*, 2019, **28**, 944–959.
- 13 A. Martinsen, G. Skjåk-Bræk, O. Smidsrød, F. Zanetti and S. Paoletti, *Carbohydr. Polym.*, 1991, **15**, 171–193.
- 14 K. Sakugawa, A. Ikeda, A. Takemura and H. Ono, *J. Appl. Polym. Sci.*, 2004, **93**, 1372–1377.
- 15 O. A. Aarstad, A. Tøndervik, H. Sletta and G. Skjåk-Bræk, *Biomacromolecules*, 2012, **13**, 106–116.
- 16 H. M. Jensen, F. H. Larsen and S. B. Engelsen, in *Natural Products From Marine Algae: Methods and Protocols*, ed. D. B. Stengel and S. Connan, Springer, 2015, 347–363.
- 17 K. I. Draget, G. Skjåk Bræk and O. Smidsrød, *Carbohydr. Polym.*, 1994, **25**, 31–38.
- 18 B. T. Stokke, O. Smidsrød, P. Bruheim and G. Skjåk-Braek, *Macromolecules*, 1991, **24**, 4637–4645.
- 19 I. Donati, S. Holtan, Y. A. Mørch, M. Borgogna and M. Dentini, *Biomacromolecules*, 2005, **6**, 1031–1040.
- 20 F. Belalia and N.-E. Djelali, *Rev. Roum. Chim.*, 2014, **59**, 135–145.
- 21 J. Ma, Y. Lin, X. Chen, B. Zhao and J. Zhang, *Food Hydrocolloids*, 2014, **38**, 119–128.
- 22 W. Jiao, W. Chen, Y. Mei, Y. Yun, B. Wang, Q. Zhong, H. Chen and W. Chen, *Molecules*, 2019, **24**, 4374.
- 23 S. Fu, A. Thacker, D. M. Sperger, R. L. Boni, I. S. Buckner, S. Velankar, E. J. Munson and L. H. Block, *AAPS PharmSci-Tech*, 2011, **12**, 453–460.
- 24 G. Xu, S. Luo, Q. Yang, J. Yang and J. Zhao, *J. Chem. Phys.*, 2016, **145**, 144903.
- 25 A. Doderò, S. Vicini, M. Alloisio and M. Castellano, *Rheol. Acta*, 2020, **59**, 365–374.
- 26 H. Storz, U. Zimmermann, H. Zimmermann and W.-M. Kulicke, *Rheol. Acta*, 2010, **49**, 155–167.
- 27 F. Hentati, G. Pierre, A. V. Ursu, C. Vial, C. Delattre, S. Abdelkafi and P. Michaud, *Food Hydrocolloids*, 2020, **103**, 105631.
- 28 R. A. Rezende, P. J. Bártolo, A. Mendes and R. M. Filho, *J. Appl. Polym. Sci.*, 2009, **113**, 3866–3871.
- 29 C. Rodríguez-Rivero, L. Hilliou, E. M. Martín del Valle and M. A. Galán, *Rheol. Acta*, 2014, **53**, 559–570.
- 30 N. Willenbacher and C. Oelschlaeger, *Curr. Opin. Colloid Interface Sci.*, 2007, **12**, 43–49.
- 31 B. Maciel, C. Oelschlaeger and N. Willenbacher, *Colloid Polym. Sci.*, 2020, **298**, 791–801.
- 32 I. P. S. Fernando, W. Lee, E. J. Han and G. Ahn, *Chem. Eng. J.*, 2020, **391**, 123823.
- 33 M. Mohammadi, M. Karimi, B. Malaekhe-Nikouei, M. Torkashvand and M. Alibolandi, *Int. J. Pharm.*, 2022, **616**, 121534.
- 34 S. Mallakpour, E. Azadi and C. M. Hussain, *Adv. Colloid Interface Sci.*, 2021, **293**, 102436.
- 35 T. Narita, K. Mayumi, G. Ducouret and P. Hébraud, *Macromolecules*, 2013, **46**, 4174–4183.
- 36 B. Chu, *Polym. J.*, 1985, **17**, 225–238.
- 37 D. Fioretto and F. Scarponi, *J. Mater. Sci. Eng. A*, 2009, **521–522**, 243–246.
- 38 G. Rohman, S. Ramtani, S. Changotade, C. Langueh, D. Lutowski, Y. Roussigné, F. Tétard, F. Caupin and P. Djemia, *Biomed. Opt. Express*, 2019, **10**, 1649–1659.
- 39 M. Choi, M. Humar, S. Kim and S.-H. Yun, *Adv. Mater.*, 2015, **27**, 4081–4086.
- 40 P. Del Gaudio, P. Colombo, G. Colombo, P. Russo and F. Sonvico, *Int. J. Pharm.*, 2005, **302**, 1–9.
- 41 T. Narayanan, M. Sztucki, P. Van Vaerenbergh, J. Léonardon, J. Gorini, L. Claustre, F. Sever, J. Morse and P. Boesecke, *J. Appl. Crystallogr.*, 2018, **51**, 1511–1524.
- 42 S.-R. Ryoo, Y.-K. Kim, M.-H. Kim and D.-H. Min, *ACS Nano*, 2010, **4**, 6587–6598.
- 43 M. McLaughlin, M. J. Earle, M. A. Gilea, B. F. Gilmore, S. P. Gorman and K. R. Seddon, *Green Chem.*, 2011, **13**, 2794–2800.
- 44 W. J. Zhang, Ch Laue, A. Hyder and J. Schrezenmeir, *Transplant. Proc.*, 2001, **33**, 3517–3519.
- 45 M. L. Torres, J. M. Fernandez, F. G. Dellatorre, A. M. Cortizo and T. G. Oberti, *Algal Res.*, 2019, **40**, 101499.
- 46 G. Klöck, H. Frank, R. Houben, T. Zekorn, A. Horcher, U. Siebers, M. Wöhrle, K. Federlin and U. Zimmermann, *Appl. Microbiol. Biotechnol.*, 1994, **40**, 638–643.
- 47 T. Andersen, P. Auk-Emblem and M. Dornish, *Microarrays*, 2015, **4**, 133–161.
- 48 D. Marani, J. Hjelm and M. Wandel, *Annu. Trans. - Nord. Rheol. Soc.*, 2013, **21**, 255–262.
- 49 M. Mancini, M. Moresi and F. Sappino, *J. Food Eng.*, 1996, **28**, 283–295.
- 50 M. Masuelli and C. Illanes, *Int. J. Biomater. Sci. Eng.*, 2014, **1**, 1–11.
- 51 A. Doderò, S. Vicini, M. Allosio and M. Castellano, *J. Mater. Sci.*, 2019, **54**, 8034–8046.
- 52 S. Roger, Y. Y. C. Sang, A. Bee, R. Perzynski, J. M. Di Meglio and A. Ponton, *Eur. Phys. J. E: Soft Matter Biol. Phys.*, 2015, **38**, 88.
- 53 S. Dou and R. H. Colby, *J. Polym. Sci., Part B: Polym. Phys.*, 2006, **44**, 2001–2013.
- 54 M. Bailey, M. Alunni-Cardinali, N. Correa, S. Caponi, T. Holsgrove, H. Barr, N. Stone, C. P. Winlove, D. Fioretto and F. Palombo, *Sci. Adv.*, 2020, **6**, eabc1937.
- 55 L. Comez, L. Lupi, M. Paolantoni, F. Picchiò and D. Fioretto, *J. Chem. Phys.*, 2012, **137**, 114509.
- 56 G. Monaco, A. Cunsolo, G. Ruocco and F. Sette, *Phys. Rev. E: Stat. Phys., Plasmas, Fluids, Relat. Interdiscip. Top.*, 1999, **60**, 5505–5521.
- 57 N. Willenbacher, C. Oelschlaeger, M. Schopferer, P. Fischer, F. Cardinaux and F. Scheffold, *Phys. Rev. Lett.*, 2007, **99**, 068302.
- 58 I. Donati and S. Paoletti, in *Alginate: Biology and Applications*, ed. B. H. A. Rehm, Springer, 2009, pp. 1–53.



- 59 H. Zhang, H. Wang, J. Wang, R. Guo and Q. Zhang, *Polym. Adv. Technol.*, 2001, **12**, 740–745.
- 60 F. Horkay, P. J. Basser, A.-M. Hecht and E. Geissler, *J. Chem. Phys.*, 2018, **149**, 163312.
- 61 Z.-Y. Wang, J. W. White, M. Konno, S. Saito and T. Nozawa, *Biopolymers*, 1995, **35**, 227–238.
- 62 M. Muthukumar, *J. Chem. Phys.*, 1996, **30**, 5183–5199.
- 63 G. Orive, A. M. Carcaboso, R. M. Hernández, A. R. Gascón and J. L. Pedraz, *Biomacromolecules*, 2005, **6**, 927–931.
- 64 R. Mihai, I. Florescu, V. Coroiu, A. Oancea and M. Lungu, *J. Med. Life*, 2011, **4**, 250–255.
- 65 M. Zborowski and J. J. Chalmers, *Magn. Cell Sep.*, 2007, **32**, 1–454.

